6-1-2019

Giant reversible barocaloric response of (MnNiSi)1- x(FeCoGe)x (x = 0.39, 0.40, 0.41)

Pol Lloveras
Universitat Politècnica de Catalunya

Tapas Samanta
Louisiana State University

María Barrio
Universitat Politècnica de Catalunya

Igor Dubenko
Southern Illinois University Carbondale

Naushad Ali
Southern Illinois University Carbondale

See next page for additional authors

Recommended Citation

Lloveras, P., Samanta, T., Barrio, M., Dubenko, I., Ali, N., Tamarit, J., & Stadler, S. (2019). Giant reversible barocaloric response of (MnNiSi)1- x(FeCoGe)x (x = 0.39, 0.40, 0.41). *APL Materials, 7* (6) https://doi.org/10.1063/1.5097959

APL Materials

Giant reversible barocaloric response of $(MnNiSi)_{1-x}(FeCoGe)_x$ (x = 0.39, 0.40, 0.41)

Cite as: APL Mater. **7**, 061106 (2019); https://doi.org/10.1063/1.5097959
Submitted: 29 March 2019 • Accepted: 03 June 2019 • Published Online: 25 June 2019

Pol Lloveras, Tapas Samanta, María Barrio, et al.

Giant reversible barocaloric response of $(MnNiSi)_{1-x}(FeCoGe)_x$ (x = 0.39, 0.40, 0.41)

Cite as: APL Mater. 7, 061106 (2019); doi: 10.1063/1.5097959
Submitted: 29 March 2019 • Accepted: 3 June 2019 •
Published Online: 25 June 2019

Pol Lloveras,[1] Tapas Samanta,[2] María Barrio,[1] Igor Dubenko,[3] Naushad Ali,[3] Josep-Lluís Tamarit,[1] and Shane Stadler[2]

AFFILIATIONS

[1]Grup de Caracterització de Materials, Departament de Física, EEBE, and Barcelona Research Center in Multiscale Science and Engineering, Universitat Politècnica de Catalunya, Campus Diagonal-Besòs, Av. Eduard Maristany, 10-14, 08019 Barcelona, Catalonia, Spain

[2]Department of Physics and Astronomy, Louisiana State University, Baton Rouge, Louisiana 70803, USA

[3]Department of Physics, Southern Illinois University, Carbondale, Illinois 62901, USA

ABSTRACT

MnNiSi-based alloys and isostructural systems have traditionally demonstrated impressive magnetocaloric properties near room temperature associated with a highly tunable first-order magnetostructural transition that involves large latent heat. However, these materials are limited by a small field-sensitivity of the transition, preventing significant reversible effects usable for cooling applications. Instead, the concomitant large transition volume changes prompt a high pressure-sensitivity, and therefore, promise substantial barocaloric performances, but they have been sparsely studied in these materials. Here, we study the barocaloric response in a series of composition-related $(MnNiSi)_{1-x}(FeCoGe)_x$ (x = 0.39, 0.40, 0.41) alloys that span continuously over a wide temperature range around ambient. We report on giant reversible effects of ~40 J K^{-1} kg^{-1} and up to ~4 K upon application of ~2 kbar and find a degradation of the first-order transition properties with pressure that limits the barocaloric effects at high pressures. Our results confirm the potential of this type of alloys for barocaloric applications, where multicaloric and composite possibilities, along with the high density and relatively high thermal conductivity, constructively add to the magnitude of the caloric effects.

I. INTRODUCTION

First-order magnetostructural transitions (FOMSTs) constitute one of the most relevant expressions within the multiferroic casuistry as they may involve an intricate network of both physical interactions and functionalities. The underlying spin-lattice coupling together with large concomitant changes in both magnitudes offers a platform where a diversity of magnetic, structural, and electronic orderings and cross-variable couplings can develop[1–5] and are at the origin of a variety of phenomena with promising technological applications such as the magnetic shape memory effect,[6] magnetic superelasticity,[7] giant magnetoresistance,[8–10] and caloric effects.[11] In particular, the latter are currently attracting great interest because they propose a clean, efficient, and down-scalable refrigeration method as an alternative to current compressors that use high-greenhouse fluids. They are based on the exchange of the latent heat associated with first-order phase transitions driven by controllable external fields. In the case of magnetocaloric (MC) materials, the latent heat in FOMSTs may entail a significant improvement of the caloric performance with respect to their second-order counterparts.[12] In addition, FOMSTs allow (i) the possibility of harvesting both magnetocaloric[11] and mechanocaloric[13] effects separately, or simultaneously, with the subsequent multicaloric advantages,[14] (ii) more compact devices as permitted by their high density, and (iii) good heat exchange due to the relatively high thermal conductivity. However, their competitiveness is restricted to the use of costless magnetic fields generated by expensive permanent magnets, which to date are limited to ~2 T.[15]

ABX-based alloys, where A and B are transition metals (typically Mn, Fe, Co, or Ni) and X is a semimetal (typically Ge or Si), are a prominent example where the occurrence of a FOMST

has revealed outstanding MC properties and rich magnetic behavior.[3,4,16,17] While MnCoGe occupies most of the attention within these types of alloys,[4,16,18–44] other structurally related compounds combining Fe, Co, Ni, and Mn, such as MnNiSi, MnNiGe, MnFeGe and CoNiGe,[2,3,19,45–52] have also deserved considerable research efforts. The occurrence of FOMSTs in these systems is, however, not ubiquitous. In the stoichiometric forms, they usually display a martensitic transition well above the Curie temperature (T_c) from a high-temperature hexagonal Ni_2In-type austenite (space group *P63/mmc*)[19,53] to a low-temperature orthorhombic TiNiSi-type martensite[54] (space group *Pnma*), with a very large volume increase of ~3%–4%. On further cooling, the orthorhombic phase undergoes a second-order ferromagnetic transition. In MnBX-based alloys, the magnetism of both structural phases basically originates from the Mn-3d band at the Fermi level,[18] with a different saturation magnetization for each phase. Recent studies have pointed to changes in the Mn-3d band originating from the increase in the Mn–Mn distances in the orthorhombic phase, which in turn destabilizes the hexagonal structure.[12,17,37]

To achieve a FOMST near room temperature, these alloys exhibit a high sensitivity of the structural transition temperature (T_0) to the specific composition that has inspired abundant studies proposing rational and systematic slight chemical changes to dramatically shift T_0 to coincide with T_c, as the latter is much less sensitive to composition variations. In this sense, an extensive literature record include the introduction of vacancies,[18,42,44] addition, or substitution by dopants.[17,24,27,29,30,32–35,37,39,40,43,45,55–57] On the other hand, the doping-induced coupling is maintained in a composition range provided that T_0 does not fall below the T_c of the hexagonal phase.[32,33,45,49,50]

As giant MC materials, these alloys present a major drawback, which is the fact that their transition temperatures appear to be little sensitive to the magnetic field, i.e., $dT/\mu_0 dH \leq 2$ K T^{-1}, compared to transition and hysteresis widths of ~10 K, as reported in literature data.[17,24,37,56] Therefore, high magnetic fields would be required to fully drive the transition and overcome the hysteresis in these materials, making them unviable for MC cooling devices. Instead, the strongly nonisochoric character of the FOMSTs occurring in such alloys makes them highly sensitive to pressure[24,56] and hence good candidates to display giant barocaloric (BC) effects,[58] but only few works have been performed so far.[52,56,57] Here, we use x-ray diffraction, magnetic measurements, and calorimetry under pressure to study the magnetostructural behavior and BC response of a series of composition-related $MnNiSi_{1-x}FeCoGe_x$ pseudobinary alloys across their FOMST occurring near room temperature. We find large and inverse BC effects that become reversible above ~0.3 kbar and reach ~50 J K^{-1} kg^{-1} at 2.5 kbar. The transition entropy change falls with pressure, thus indicating a weakening of the first-order character and a decrease of the BC performance at low temperature.

FeCoGe stabilizes in the hexagonal structure at any temperature, with T_c at 370 K.[52] MnNiSi is isostructural above 1200 K, whereas at this temperature, it transforms to the orthorhombic structure.[19] Therefore, in the $MnNiSi_{1-x}FeCoGe_x$ pseudobinary alloy, it is reasonable to state that the FeCoGe elements provoke the stabilization of the hexagonal phase down to lower temperatures and may lead to a coupled magnetostructural transition. For the analyzed compositions $x = 0.39$, 0.40, and 0.41, a FOMST takes place from hexagonal paramagnetic to orthorhombic ferromagnetic around room temperature.

II. EXPERIMENTAL DETAILS

Polycrystalline $(MnNiSi)_{1-x}(FeCoGe)_x$ (x = 0.39, 0.40, and 0.41) samples were prepared by melting the constituent elements of >99.9% purity in an ultra-high purity Ar atmosphere using an RF-furnace. X-ray diffraction measurements were performed using Cu-K_α radiation (λ = 1.5406 Å) to determine both the phase purity of the samples and the temperature-dependent lattice parameters with the diffractometers described in Refs. 52 and 57, respectively. Pattern matching has been performed using FullProf software.[59] Magnetization measurements at normal pressure and under high hydrostatic pressure were performed as described in Ref. 52. Calorimetric measurements at normal pressure were carried out using a commercial Differential Scanning Calorimeter Q100 from TA Instruments, whereas calorimetry under hydrostatic pressure was performed employing the custom-built Cu-Be calorimeter and methods described in Ref. 58. Temperature rates were typically of ~2 K min^{-1}.

III. RESULTS

X-ray measurements confirm the expected hexagonal-to-orthorhombic structural change for the three compounds [see Figs. S1(a)–S1(c) of the supplementary material]. The cell parameters of each phase [Figs. S2(a)–S2(c) of the supplementary material], as obtained from pattern matching, are basically insensitive to the slight differences in composition and reveal a finite and large volume expansion of about 2.7%–2.8% on cooling across the first-order phase transformation [Fig. 1(a) and Figs. S2(d)–S2(f) of the supplementary material]. In contrast, the transition temperatures decrease significantly with increasing FeCoGe content, consistent with the role of this subsystem in favoring the stabilization of the hexagonal phase. On the other hand, the temperature-dependent volume indicates a small thermal expansion $\alpha = (1/V)(\partial V/\partial T)_p$ in each side of the transition, anticipating negligible BC effects outside the transition [for x = 0.39, $\alpha_{Hex} = (3.4 \pm 0.2) \times 10^{-5}$ K^{-1} and $\alpha_{Orth} = (2.0 \pm 0.2) \times 10^{-5}$ K^{-1}; for x = 0.40, $\alpha_{Hex} = (3.4 \pm 0.2) \times 10^{-5}$ K^{-1} and $\alpha_{Orth} = (2.3 \pm 0.2) \times 10^{-5}$ K^{-1}; and for x = 0.41, $\alpha_{Hex} = (5.0 \pm 0.2) \times 10^{-6}$ K^{-1} and $\alpha_{Orth} = (4.9 \pm 0.2) \times 10^{-5}$ K^{-1}]. The small volume variations with temperature of each phase but very large volume differences between phases are likely at the origin of the mechanical failure and subsequent powderization of the bulk samples when crossing the transition for the first time, which contrasts with the large hardness of the samples outside the transition. This behavior has been widely observed in alloys isostructural to those studied here and has been associated with the occurrence of the virgin effect.[48,50,60–66]

The temperature evolution of the magnetization under 0.1 T [see Fig. 1(b)] for the three different compositions shows a sharp and hysteretic change at the transition, indicating the concurrent magnetic character of the first-order structural transformation. Magnetization at 5 T [see Fig. 1(b)] at normal and high pressure [see Fig. 1(c) for x = 0.40] indicates that the dependence of the transition temperature on the magnetic field is small and largely independent of composition and applied pressure [$dT/\mu_0 dH$ ~ 1.2 K T^{-1},

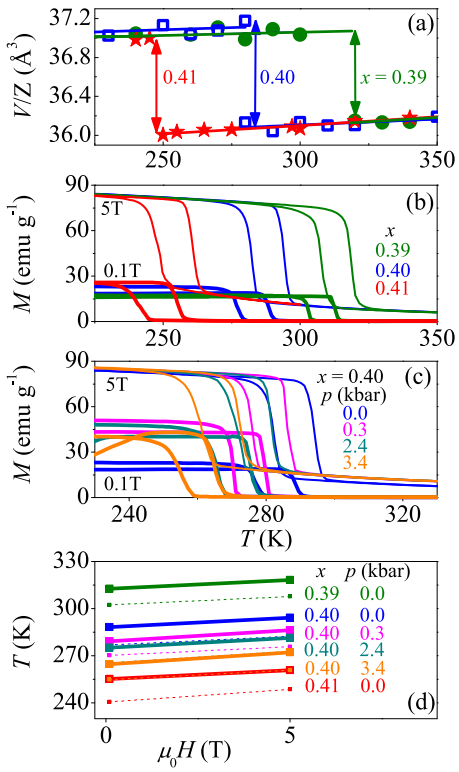

FIG. 1. (a) Volume per formula unit as a function of temperature obtained from x-ray diffraction for the different compositions. (b) Temperature-dependent magnetization under $\mu_0 H$ = 0.1 and 5 T fields for the three different compositions. (c) Temperature-dependent magnetization for the composition x = 0.40 under different pressures. (d) Temperature-magnetic field phase diagram for the different compositions and pressures, as derived from (b) and (c).

see Fig. 1(d)]. This suggests that a magnetic field of ~9 T should be applied to overcome a ~11 K of hysteresis and thus achieve reversible MC effects, which are prohibitively excessive for applications as anticipated previously. Second, for completeness, it is worth mentioning the presence of a hysteretic decrease of the magnetization observed on further cooling the x = 0.40 sample under 2.4 and 3.4 kbar. It indicates the presence of another first-order magnetic transition at low temperatures, which could be contributed by antiferromagnetic interactions, as reported in similar alloys.[4,16,20,29,45,47]

Temperature-dependent heat flow $dQ/|dT|$ at atmospheric pressure for the different compositions (see Fig. S3 of the supplementary material) displays exothermic (negative) peaks on cooling corresponding to the forward martensitic transition (hereafter M) from the hexagonal austenite toward the orthorhombic martensite and endothermic (positive) peaks on heating corresponding to the backward transition (hereafter A). Defining the transition temperature as the temperature at which 50% of the material is transformed, we find that the forward and backward transition temperatures, T_M and T_A, depend on composition x as $dT_M/(100dx) = -30 \pm 2$ K and $dT_A/(100dx) = -27 \pm 2$ K. Integration of the peaks after baseline subtraction renders the forward and backward enthalpy ($|\Delta H_M|$ and $|\Delta H_A|$) and entropy changes ($|\Delta S_M|$ and $|\Delta S_A|$), and are listed in Table I, revealing large changes compared to other magnetic alloys.[1,58,67–73]

Temperature-dependent heat flow $dQ/|dT|$ data at high pressures for the different compositions are shown in Figs. 2(a)–2(c). In all cases, both endothermic and exothermic peaks shift to lower temperatures when the applied pressure is increased. This behavior indicates a consistent enhancement of the stable temperature range of the lower-volume hexagonal phase at higher pressures and implies inverse BC effects.[67] Figure 2(d) shows the forward and backward transition temperatures, T_M and T_A, as a function of pressure for the different compositions ($dT/dp < 0$; see Table I). The colored regions around each temperature-pressure transition line indicate the transition width, limited by the starting and finishing temperatures for the forward (M_s and M_f, respectively) and backward (A_s and A_f, respectively) martensitic transitions. From this plot, the minimum pressure leading to reversible isothermal entropy changes ΔS can be determined as the pressure at which A_s at high pressure equals M_s at normal pressure.[74] In all cases, this value remains well below the modest pressure of 1 kbar, thus prognosticating a very good reversibility.

Integration of the calorimetric peaks $(1/T)(dQ/|dT|)$ after baseline subtraction renders pressure-dependent entropy changes at the transition [$\Delta S_i(p)$ with i = M, A hereafter standing for the forward and reverse martensitic transition, respectively], as shown in Figs. 2(e)–2(g) for the different compositions. The pressure-dependent enthalpy changes $\Delta H_i(p)$ and volume changes $\Delta V_i(p)$ as calculated via Clausius-Clapeyron, $\Delta V_i(p) = \Delta S_i(p)(dT_i/dp)$ (i = M, A) are shown in Fig. S4 of the supplementary material. The values of T_i, ΔH_i, and ΔS_i at normal pressure as a function of composition x are displayed in Figs. S5(a)–S5(c) of the supplementary material, whereas the transition volume change ΔV_i at normal pressure as a function of composition both calculated from Clausius-Clapeyron and experimentally determined from x-ray diffraction are displayed

TABLE I. Thermodynamic data for $(MnNiSi)_{1-x}(FeCoGe)_x$ samples: Temperatures, entropy, and enthalpy changes and temperature-pressure slopes for the forward (M) and backward (A) transformations, and volume changes (determined from x-ray measurements).

x	T_A (K)	T_M (K)	$\lvert\Delta S_A\rvert$ (J K^{-1} kg^{-1})	$\lvert\Delta S_M\rvert$ (J K^{-1} kg^{-1})	$\lvert\Delta H_A\rvert$ (J K^{-1} kg^{-1})	$\lvert\Delta H_M\rvert$ (J K^{-1} kg^{-1})	dT_A/dp (K kbar^{-1})	dT_M/dp (K kbar^{-1})	$\Delta V \times 10^{-3}$ (cm^3 g^{-1})
0.39	313 ± 1	309 ± 1	62 ± 2	64 ± 2	19 ± 1	19 ± 1	−7.0 ± 0.1	−6.9 ± 0.3	3.6 ± 0.4
0.40	286 ± 1	274 ± 1	61 ± 2	65 ± 2	18 ± 1	18 ± 1	−7.7 ± 0.4	−6.8 ± 0.3	3.9 ± 0.4
0.41	254 ± 1	240 ± 1	54 ± 2	57 ± 2	14 ± 1	14 ± 1	−7.8 ± 0.1	−7.1 ± 0.2	3.7 ± 0.4

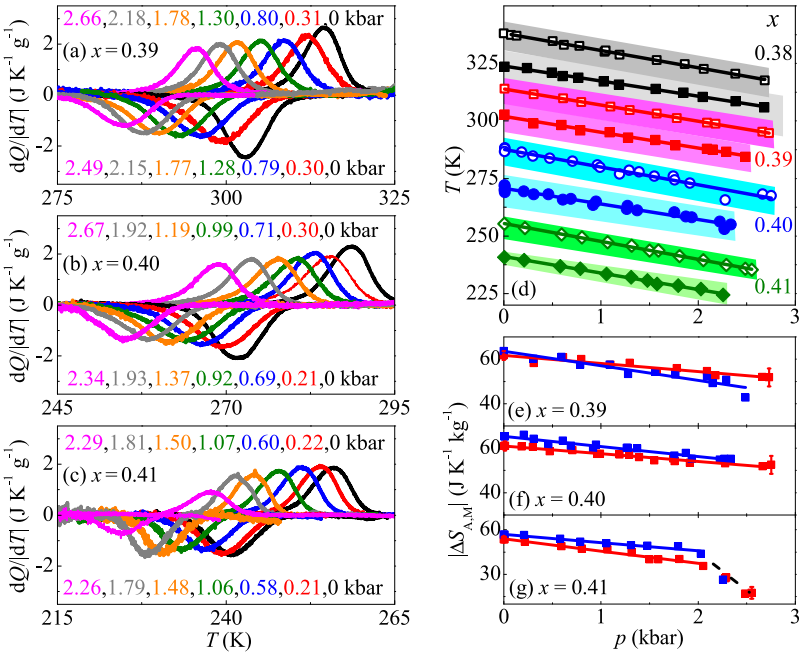

FIG. 2. Heat flow as a function of temperature at different selected pressures on heating (positive) and cooling (negative) for the different compositions: (a) x = 0.39, (b) x = 0.40, and (c) x = 0.41. Pressure values are indicated above each peak. (d) Transition temperature on heating (empty symbols) and cooling (solid symbols) as a function of pressure. Colored stripes stand for the average transition temperature range at each pressure obtained from fits of the starting (A_s and M_s) and finishing (A_f and M_f) transition temperatures as indicated for the sample x = 0.40. For completeness, data for x = 0.38 from Ref. 52 are also shown, including unpublished starting and finishing temperatures. [(e)–(g)] Pressure-dependent entropy changes across the forward (ΔS_M, blue squares) and backward transitions (ΔS_A, red squares) for the different compositions. Lines are linear regressions to the data. For x = 0.41, data at $p > 2$ kbar have not taken into account in the linear fits as they fall out of the trend obtained at lower pressures, as indicated by the black dashed line.

in Fig. S5(d) of the supplementary material. Interestingly, by considering also the negative sign of the pressure-derivatives dT_i/dp, $d|\Delta H_i|/dp$, $d|\Delta S_i|/dp$, and $d|\Delta V_i|/dp$, [as shown in Figs S5(e)–S5(h) of the supplementary material], one can conclude that both increasing p or x have a similar effect of causing a decrease in all the aforementioned quantities. This is consistent with the fact that both p and x favor the stabilization of the lower-volume austenite phase and has led to denote similar variations in compositions as *chemical*

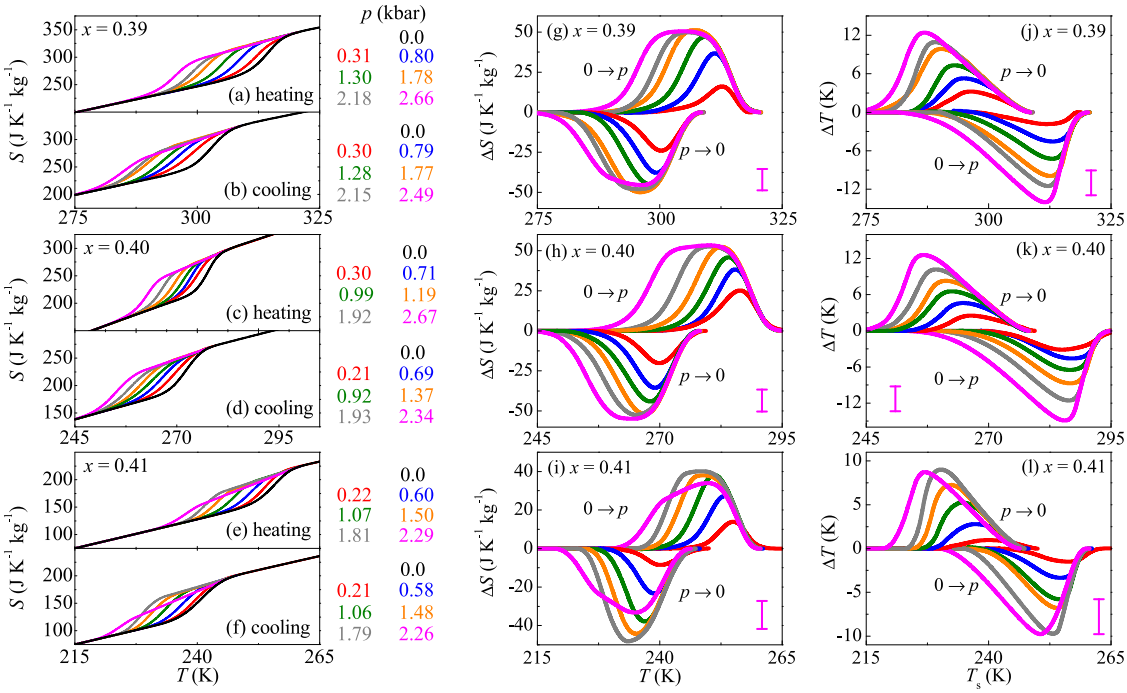

FIG. 3. [(a)–(f)] Isobaric entropy curves with respect to a reference entropy at 180 K for the 3 different compositions. [(g)–(l)] Barocaloric effects for the different compositions. [(g)–(i)] Isothermal entropy changes as function of temperature for different applied pressures. [(j)–(l)] Adiabatic temperature changes as function of the start temperature for different applied pressures. Changes on applying pressure were calculated from heating runs [(a), (c), and (e)] and changes on removing pressure were calculated from cooling runs [(b), (d), and (f)].

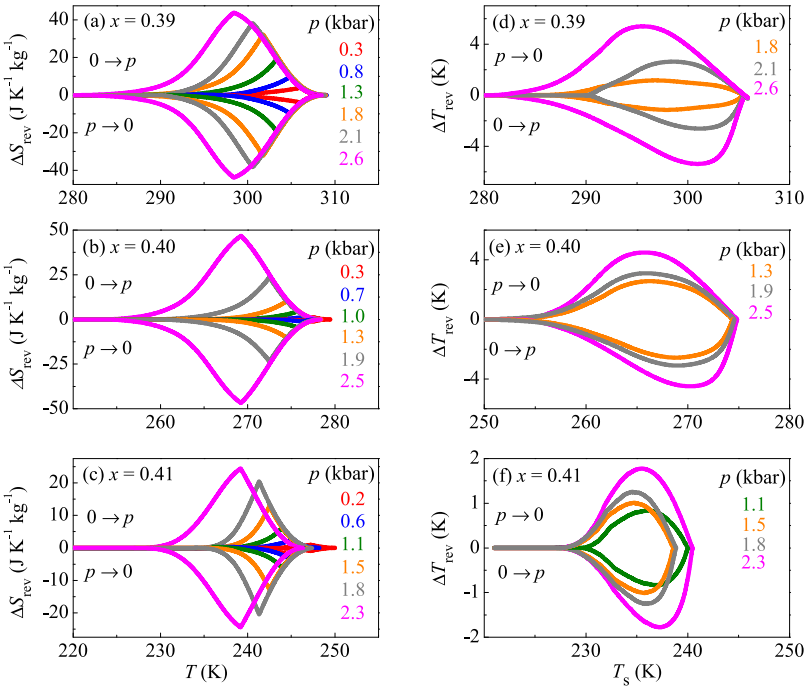

FIG. 4. Reversible barocaloric effects for the different compositions. [(a)–(c)] Reversible isothermal entropy changes. [(d)–(f)] Reversible adiabatic temperature changes.

pressure.[12,22,37,44,51,56] In B-doped MnCoGe[39] and other isostructural alloys, it has been observed that lowering the transition temperature may lead to the emergence and/or increase of the retained fraction of the hexagonal structure within the orthorhombic phase. As pressure also decreases the transition temperature, it would become reasonable to consider that the fall of $|\Delta H_i(p)|$ [and $|\Delta S_i(p)|$] with pressure might be explained as due to an increase of the retained hexagonal fraction. To rule out this hypothesis, we have

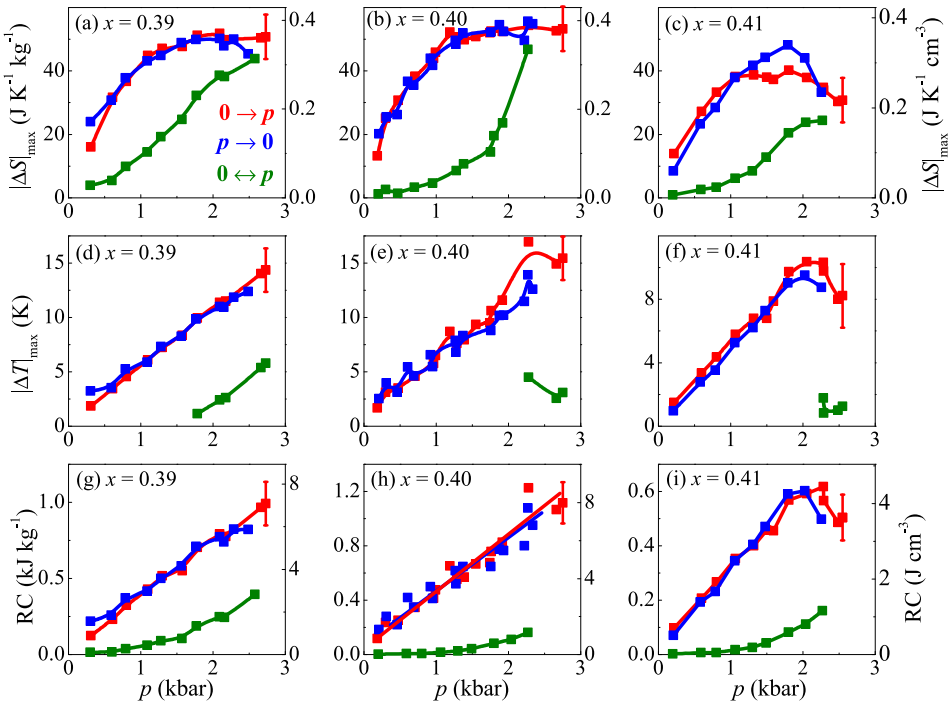

FIG. 5. [(a)–(c)] Maximum ΔS, [(d)–(f)] maximum ΔT and [(g)–(i)] refrigeration capacity (RC) as a function of applied pressure on irreversible (red for compressions and blue for decompressions) and reversible (green) processes. For $|\Delta S|_{max}$ and RC, values per unit mass (left axis) and unit volume (right axis) are shown.

TABLE II. Summary of barocaloric results for $(MnNiSi)_{1-x}(FeCoGe)_x$ samples extracted from Fig. 5.

x	$\lvert\Delta S\rvert$ (J K^{-1} kg^{-1})	$\lvert\Delta S\rvert$ (J K^{-1} cm^{-3})	$\lvert\Delta T\rvert$ (K)	$\lvert\Delta S_{rev}\rvert$ (J K^{-1} kg^{-1})	$\lvert\Delta S_{rev}\rvert$ (J K^{-1} cm^{-3})	$\lvert\Delta T_{rev}\rvert$ (K)	p (kbar)
0.39	52 ± 5	0.37 ± 0.04	14 ± 2	44 ± 5	0.31 ± 0.04	6 ± 2	2.6
0.40	54 ± 5	0.38 ± 0.04	17 ± 2	47 ± 5	0.33 ± 0.04	4 ± 2	2.3
0.41	40 ± 5	0.28 ± 0.04	10 ± 2	24 ± 5	0.17 ± 0.04	1.8 ± 2	2.3

performed measurements on heating at high pressure after cooling at normal pressure (zero-pressure-cooling, ZPC) and after cooling at high pressure (pressure-cooling, PC) [see Figs. S6(a) and S6(b) for the protocol, Fig. S6(c) for the thermograms, and Fig. S6(d) for the resulting $|\Delta H_i(p)|$ in the supplementary material]. As $\Delta H_i(p)$ values are history-independent, the decrease in $|\Delta H_i(p)|$ with pressure cannot be explained by a pressure-dependent transformed fraction but should be associated with a weakening of the transition, similarly to the observed behavior in similar systems.[33,44,56] On the other hand, for $x = 0.41$ and $p > 2$ kbar, it is observed that a dramatic drop in $|\Delta H_i(p)|$ and $|\Delta S_i(p)|$, as suggested by previous observations in isostructural systems,[20,22,24,26,27,32,33,44,56] could be originated by the fact that the shift of the transition to lower temperatures due to composition and pressure brings the system to fall below the low-temperature limit of the range where magnetostructural coupling occurs. Consequently, such pressure-induced decoupling[24] leads the transition entropy change to lose a significant contribution coming from a (partial) magnetic ordering.

The isobaric entropy curves required to determine the BC effects were calculated with respect to a reference entropy at $T = 180$ K [see Figs. 3(a)–3(f)] following Ref. 72 from the pressure-dependent integrations across the transition and considering the heat capacity C_p (taken from Ref. 52) to be independent of composition and pressure. The latter assumption is consistent with the fact that additional entropy changes outside the transition, as calculated from the Maxwell relation $\Delta S_+ = -\int(\partial V/\partial T)_p dp$,[75] can be safely neglected because the small thermal expansion of both phases renders $|\Delta S_+| < 1.5 \pm 1$ J K^{-1} kg^{-1} under an increase of $\Delta p \sim 2.5$ kbar,

TABLE III. Maximum reversible BC effects in solids reported in the literature and this work. ΔS_{rev} stands for maximum reversible isothermal entropy changes per unit mass and per unit volume, and ΔT_{rev} stands for maximum reversible adiabatic temperature changes upon cyclic application and removal of pressure p. Transition temperature T and pressure-dependent derivative dT/dp are averaged over heating and cooling values. *Peak hyst.* and *Onset hyst.* stand for hysteresis width as derived from the position of the peak temperature and of the onset temperature, respectively, and are useful to estimate the minimum pressure for which ΔS_{rev} and ΔT_{rev} can be obtained. Dots stand for unreported data.

Compound	T (K)	dT/dp (K kbar^{-1})	Peak hyst. (K)	Onset hyst. (K)	$\lvert\Delta S_{rev}\rvert$ (J K^{-1} kg^{-1})	$\lvert\Delta S_{rev}\rvert$ (J K^{-1} cm^{-3})	$\lvert\Delta T_{rev}\rvert$ (K)	p (kbar)	References
$Ni_{49.26}Mn_{36.08}In_{14.66}$	293	1.8	...	...	10	0.082	...	2.5	76
$Ni_{2.02}Mn_{1.36}In_{0.62}$	346	1.83	4	0	10	0.082	...	2.5	71
$Ni_{2.05}Mn_{1.30}In_{0.65}$	330	1.65	6	0	5	0.041	...	2.5	71
$Ni_{1.99}Mn_{1.37}In_{0.64}$	329	1.95	4	0	6	0.049	...	2.5	71
$Ni_{1.99}Mn_{1.34}In_{0.67}$	306	1.37	3	0	4	0.033	...	2.0	71
$Ni_{2.00}Mn_{1.32}In_{0.68}$	275	1.88	5	0	4	0.033	...	2.5	71
$Fe_{49}Rh_{51}$	308	6	10	5	12.4	0.12	5	2.4	70 and 72
$BaTiO_3$	400	−5.6	4	0	1.47	0.0088	...	1.2	77
$(NH_4)_2(SO)_4$	219	−5	4	0	57.5	0.10	...	1.5	75
[TPrA][Mn(dca)$_3$]	330	23.1	0.9	...	32.9	0.041	...	0.07	78
[TPrA][Cd(dca)$_3$]	330	38.2	1.4	...	11.5	0.016	...	0.07	79
V-N rubber[a]	300	...	...	...	...	...	11	1.73	80
PDMS rubber[a]	283	...	...	...	...	...	28	3.9	81
N-B rubber[a]	314	...	...	...	59	0.082	16.4	3.9	82
AgI	420	−13.5	25	14	58.6	0.33	17	2.5	76
Neopentylglycol	314	10	20	13	510	0.54	25	5.7	83
$[FeL_2][BF_4]_2$	262	10	4	1	...	...	6	1	84
$(MnNiSi)_{0.62}(FeCoGe)_{0.38}$	338	−7.5	...	...	57	0.42	...	2.7	52
$(MnNiSi)_{0.61}(FeCoGe)_{0.39}$	311	−7.0	4	1	44	0.31	6	2.6	This work
$(MnNiSi)_{0.60}(FeCoGe)_{0.40}$	280	−7.7	12	4	47	0.33	4	2.3	This work
$(MnNiSi)_{0.59}(FeCoGe)_{0.41}$	247	−7.8	14	6	24	0.17	1.8	2.3	This work

[a]Materials with large BC effects that are not related with first-order phase transitions.

which falls within the errors of our entropy calculations. In addition, we have checked that unexpected errors as large as 25% in the values of C_p would yield variations of up to 7% in the values of ΔT and ΔT_{rev} at the maximum applied pressure of 2.6 kbar (see Fig. S7 of the supplementary material), which also fall within the given uncertainties, whereas ΔS and ΔS_{rev} would approximately remain invariant.

BC effects were calculated according to the quasidirect method as subtraction between isobaric curves at different pressures following proper paths, i.e., isothermal entropy changes were calculated as $\Delta S(T, \Delta p) = S(T, p_f) - S(T, p_0)$ and adiabatic temperature changes were calculated as $\Delta T(S, \Delta p) = T(S, p_f) - T(S, p_0)$, where the lower pressure value has always been taken as normal pressure. Because of the inverse ($dT_i/dp < 0$) and mainly athermal (hysteresis rate-independent) character of the transition, the transition line crossed on compression (decompression) coincides with the transition line crossed on heating (cooling). Consequently, both ΔS and ΔT on compression (decompression) have been calculated from the isobaric curves on heating (cooling) and are shown in Figs. 3(g)–3(i) and Figs. 3(j)–3(l), respectively. Reversible entropy changes $|\Delta S_{rev}|$, computed from the overlapping between the irreversible ΔS on compression and decompression[74] [see Figs. 4(a)–4(c)], are already obtained at very low pressures $p \geq 0.3$ kbar and reach giant values at higher pressures that become even more relevant when normalized per unit volume given the high density of the compounds ($\rho \sim 7.2$ g cm^{-3}). Reversible adiabatic temperature changes $|\Delta T_{rev}|$ were computed from subtraction of the isobaric curve on heating at high pressure from the isobaric curve on cooling at normal pressure following adiabatic paths[76] [see Figs. 4(d)–4(f)]. Maximum irreversible and reversible BC effects and refrigeration capacity (RC)[75] as a function of pressure are shown in Fig. 5, with values for ΔS and RC per unit mass (left axis) and unit volume (right axis). Our results, summarized in Table II, place our alloy family amongst the best reversible BC materials reported so far near room temperature (a comparison is given in Table III).

IV. DISCUSSION

Rough estimates used to predict good caloric materials habitually come from transition entropy changes at normal pressure $\Delta S \sim \Delta S_i(p_{atm})$ and the field-sensitivity of the transition temperature, $\Delta T \sim (dT_i/dp)\Delta p$. In the present case, however, and despite our giant values, we obtain $\Delta S < \Delta S_i(p_{atm})$ and $\Delta T < (dT_i/dp)\Delta p$. This is due to the nontrivial decrease of the transition entropy change when increasing pressure as revealed by our high-pressure calorimetry, which demonstrates the importance of this technique for a proper BC characterization. Otherwise, assuming a pressure-independent transition entropy change as done elsewhere[56] may give rise to large inaccuracies or incorrect conclusions. Our observed decrease can be explained by the contributions of two factors: On one hand, as shown in Ref. 85, the isobaric entropy of the hexagonal phase decreases more rapidly with decreasing temperature than the isobaric entropy of the orthorhombic phase. As a result, the shift of the transition to lower temperatures results in a decrease of the entropy difference between the two phases, assuming that pressure dependence on the entropy is much weaker than the temperature dependence. On the other hand, it is widely accepted that the fact that the T_c of both phases exhibits much smaller sensitivity to pressure and composition than the structural transition leads the magnetostructural coupling to occur only in a temperature range nearly limited by the T_c of the two phases.[32,33,45,49,50] Therefore, the application of pressure may eventually shift the FOMST temperature below the T_c of the hexagonal phase, resulting in a (partial) decoupling of the structural from the magnetic transition.[24] Subsequently, this decoupling entails a decrease of the entropy change and the weakening of the first-order character of the surviving transition. This is further supported by experimental evidences reported elsewhere in temperature-dependent magnetization measurements at some specific values of composition and/or at high pressure, that reveal either a smoothing of the magnetization change across the transition or a two-stage transition, a second-order step followed by a first-order step.[20,22,24,26,27,32,33,44]

V. SUMMARY AND CONCLUSIONS

Our study demonstrates the great barocaloric potential near room temperature and at moderate pressures of some magnetic alloys that are also less expensive than those containing Gd. They offer an alternative to the MC effects traditionally reported in the same and similar alloys that would require too large and expensive magnetic fields to achieve reversibility. The values of the giant BC effects in our MnNiSi-FeCoGe alloys are amongst the largest BC effects reported for magnetic materials. Although they are smaller than the largest BC effects observed in nonmagnetic materials, magnetostructural alloys should not be left behind in an integral BC research as, in addition to a notable reversible BC response, they offer additional significant advantages that compare favorably to other systems with larger BC effects, as clearly set out by our work: (i) fine tuning of operational temperatures via doping that enables the fabrication of composites with a very wide temperature span using close-composition alloys, and (ii) high density which improves the compactness. Also, a relatively large thermal conductivity improves the heat transfer efficiency and the possibility of multicaloric effects through the simultaneous or successive application of mechanical and magnetic fields allows the enhancement of the reversible operational range and other multicaloric advantages.

SUPPLEMENTARY MATERIAL

See supplementary material for selected x-ray diffraction patterns, lattice parameters and volume over a wide temperature range, conventional differential scanning calorimetry at atmospheric pressure, pressure-dependent and composition-dependent transition thermodynamic quantities, and details about the protocol to check the pressure-independence of the transformed fraction and propagation of errors derived from C_p.

ACKNOWLEDGMENTS

This work was supported by MINECO, Project No. FIS2017-82625-P, and AGAUR, DGU Project No. 2017SGR-42, and by the U.S. Department of Energy (DOE), Office of Science, Basic Energy Sciences (BES) under Award Nos. DE-FG02-13ER46946 (LSU) and DE-FG02-06ER46291 (SIU).

REFERENCES

[1] D. Boldrin, E. Mendive-Tapia, J. Zemen, J. B. Staunton, T. Hansen, A. Aznar, J.-L. Tamarit, M. Barrio, P. Lloveras, J. Kim, X. Moya, and L. F. Cohen, Phys. Rev. X **8**, 041035 (2018).
[2] S. Anzai and K. Ozawa, Phys. Rev. B **18**, 2173 (1978).
[3] A. Barcza, Z. Gercsi, K. S. Knight, and K. G. Sandeman, Phys. Rev. Lett. **104**, 247202 (2010).
[4] Z. Gercsi, K. Hono, and K. G. Sandeman, Phys. Rev. B **83**, 174403 (2011).
[5] A. Singh, V. Pandey, R. K. Kotnala, and D. Pandey, Phys. Rev. Lett. **101**, 247602 (2008).
[6] R. Kainuma, Y. Imano, W. Ito, Y. Suton, H. Morito, S. Okamoto, O. Kitakami, A. F. K. Oikawa, T. Kanomata, and K. Ishida, Nature **439**, 957 (2006).
[7] K. Ullakko, J. K. Huang, and C. Kanter, J. Appl. Phys. **81**, 5416 (1997).
[8] E. Dagotto, T. Hotta, and A. Moreo, Phys. Rep. **344**, 1 (2001).
[9] J. Mira and J. Rivas, Mod. Phys. Lett. B **18**, 725 (2004).
[10] S. Pandey, A. Quetz, A. Aryal, I. Dubenko, D. Mazumdar, S. Stadler, and N. Ali, Magnetochemistry **3**, 3 (2017).
[11] X. Moya, S. Kar-Narayan, and N. D. Mathur, Nat. Mater. **13**, 439 (2014).
[12] F. Guillou, F. Wilhelm, O. Tegus, and A. Rogalev, Appl. Phys. Lett. **108**, 122405 (2016).
[13] L. Mañosa and A. Planes, Adv. Mater. **29**, 1603607 (2017).
[14] E. Stern-Taulats, T. Castán, L. Mañosa, A. Planes, N. D. Mathur, and X. Moya, MRS Bull. **43**, 295 (2018).
[15] V. K. Pecharsky, J. Cui, and D. D. Johnson, Philos. Trans. R. Soc., A **374**, 20150305 (2016).
[16] T. Samanta, I. Dubenko, A. Quetz, J. Prestigiacomo, P. A. Adams, S. Stadler, and N. Ali, Appl. Phys. Lett. **103**, 042408 (2013).
[17] S. Lin, O. Tegus, E. Brück, W. Dagula, T. J. Gortnemulder, and K. H. J. Buschow, IEEE Trans. Magn. **42**, 3776 (2006).
[18] T. Kanomata, H. Ishigaki, T. Suzuki, H. Yoshida, S. Abe, and T. Kaneko, J. Magn. Magn. Mater. **140-144**, 131 (1995).
[19] V. Johnson, Inorg. Chem. **14**, 1117 (1975).
[20] E. K. Liu, W. Zhu, L. Feng, J. L. Chen, W. H. Wang, G. H. Wu, H. Y. Liu, F. B. Meng, H. Z. Luo, and Y. X. Li, Europhys. Lett. **91**, 17003 (2010).
[21] K. Koyama, M. Saka, T. Kanomata, and K. Watanabe, Jpn. J. Appl. Phys., Part 1 **43**, 8036 (2004).
[22] Y.-Y. Zhao, F.-X. Hu, L.-F. Bao, J. Wang, H. Wu, Q. Huang, R. Wu, Y. Liu, F.-R. Shen, H. Kuang, M. Zhang, W.-L. Zuo, X.-Q. Zheng, J. R. Sun, and B.-G. Shen, J. Am. Chem. Soc. **137**, 1746 (2015).
[23] N. Hassan, F. Chen, M. Zhang, I. Ahmad, S. J. Liu, Y. Gong, G. Xu, and F. Xu, J. Magn. Magn. Mater. **439**, 120–125 (2017).
[24] L. Caron, N. T. Trung, and E. Brück, Phys. Rev. B **84**, 020414(R) (2011).
[25] J. L. Wang, P. Shamba, W. D. Hutchison, M. F. Md Din, Q. Y. Ren, Z. X. Cheng, S. J. Kennedy, S. J. Campbell, and S. X. Dou, J. Appl. Phys. **117**, 17D03 (2015).
[26] T. Samanta, I. Dubenko, A. Quetz, S. Stadler, and N. Ali, J. Appl. Phys. **113**, 17A922 (2013).
[27] J. L. Wang, P. Shamba, W. D. Htuchison, M. F. Md Din, J. C. Debnath, M. Avdeev, R. Zeng, S. J. Kennedy, S. J. Campbell, and S. X. Dou, J. Alloys Compd. **577**, 475–479 (2013).
[28] T. Samanta, I. Dubenko, A. Quetz, S. Stadler, and N. Ali, Appl. Phys. Lett. **101**, 242405 (2012).
[29] N. T. Trung, V. Biharie, L. Zhang, L. Caron, K. H. J. Buschow, and E. Brück, Appl. Phys. Lett. **96**, 162507 (2010).
[30] P. Shamba, J. L. Wang, J. C. Debnath, S. J. Kennedy, R. Zeng, M. F. Md Din, F. Hong, Z. X. Cheng, A. J. Studer, and S. X. Dou, J. Phys.: Condens. Matter **25**, 056001 (2013).
[31] L. F. Bao, F. X. Hu, R. R. Wu, J. Wang, L. Chen, J. R. Sun, B. G. Shen, L. Li, B. Zhang, and X. X. Zhang, J. Phys. D: Appl. Phys. **47**, 055003 (2014).
[32] D. Choudhury, T. Suzuki, Y. Tokura, and Y. Taguchi, Sci. Rep. **4**, 7544 (2014).
[33] D. Zhang, Z. Nie, Z. Wang, L. Huang, Q. Zhang, and Y. Wang, J. Magn. Magn. Mater. **387**, 107 (2015).
[34] Q. Y. Ren, W. D. Hutchison, J. L. Wang, A. J. Studer, M. F. Md Din, S. Muñoz-Pérez, J. M. Cadogan, and S. J. Campbell, J. Phys. D: Appl. Phys. **49**, 175003 (2016).
[35] A. Aryal, A. Quetz, S. Pandey, I. Dubenko, S. Stadler, and N. Ali, Adv. Condens. Matter Phys. **2017**, 2683789.
[36] Y. Shen and Y. Liu, Mater. Res. Express **4**, 116110 (2017).
[37] Q. Y. Ren, W. D. Hutchison, J. L. Wang, A. J. Studer, and S. J. Campbell, J. Alloys Compd. **693**, 32–39 (2017).
[38] F. X. Liang, F. R. Shen, Y. Liu, K. M. Qiao, J. Wang, F. X. Hu, J. R. Sun, and B. G. Shen, AIP Adv. **8**, 056417 (2018).
[39] N. T. Trung, L. Zhang, L. Caron, K. H. J. Buschow, and E. Brück, Appl. Phys. Lett. **96**, 172504 (2010).
[40] T. Gao, M. Wu, N. Qi, T. Zhou, X. Luo, Y. Liu, K. Xu, V. V. Marchenkov, H. Dong, Z. Chen, and B. Chen, J. Alloys Compd. **753**, 149 (2018).
[41] X. Si, Y. Liu, X. Lu, Y. Shen, W. Wang, W. Yu, T. Zhou, and T. Gao, J. Appl. Phys. **121**, 185103 (2017).
[42] Y. K. Fang, C. C. Yeh, C. W. Chang, W. C. Chang, M. G. Zhu, and W. Lib, Scr. Mater. **57**, 453 (2007).
[43] J. W. Lai, Z. G. Zheng, R. Montemayor, X. C. Zhong, Z. W. Liu, and D. C. Zeng, J. Magn. Magn. Mater. **372**, 86 (2014).
[44] Y. Liu, M. Zhang, F. Hu, J. Wang, R. Wu, Y. Zhao, H. Kuang, W. Zuo, J. Sun, and B. Shen, IEEE Trans. Magn. **51**, 2504704 (2015).
[45] A. Quetz, T. Samanta, I. Dubenko, M. J. Kangas, J. Y. Chan, S. Stadler, and N. Ali, J. Appl. Phys. **114**, 153909 (2013).
[46] T. Samanta, I. Dubenko, A. Quetz, S. Temple, S. Stadler, and N. Ali, Appl. Phys. Lett. **100**, 052404 (2012).
[47] K. Xu, Z. Li, E. Liu, H. Zhou, Y. Zhang, and C. Jing, Sci. Rep. **7**, 41675 (2017).
[48] D. T. Cam Thanh, E. Brück, O. Tegus, J. C. P. Klaasse, T. J. Gortenmulder, and K. H. J. Buschow, J. Appl. Phys. **99**, 08Q107 (2006).
[49] J. Liu, Y. Gong, G. Xu, G. Peng, I. Ahmad Shah, N. Hassan, and F. Xu, Sci. Rep. **6**, 23386 (2016).
[50] C. L. Zhang, H. F. Shi, E. J. Ye, Y. G. Nie, Z. D. Han, B. Qian, and D. H. Wang, Appl. Phys. Lett. **107**, 212403 (2015).
[51] T. Samanta, D. L. Lepkowski, A. Us Saleheen, A. Shankar, J. Prestigiacomo, I. Dubenko, A. Quetz, I. W. H. Oswald, G. T. McCandless, J. Y. Chan, P. W. Adams, D. P. Young, N. Ali, and S. Stadler, Phys. Rev. B **91**, 020401(R) (2015).
[52] T. Samanta, P. Lloveras, A. Us Saleheen, D. Lepkowski, E. Kramer, I. Dubenko, P. Adams, D. Young, M. Barrio, J.-L. Tamarit, N. Ali, and S. Stadler, Appl. Phys. Lett. **112**, 021907 (2018).
[53] W. Jeitschko, Acta Crystallogr., Sect. B: Struct. Crystallogr. Cryst. Chem. **31**, 1187 (1975).
[54] C. B. Shoemaker and D. P. Shoemaker, Acta Crystallogr. **18**, 900 (1965).
[55] A. Quintana-Nedelcos, J. L. Sánchez Llamazares, and H. Flores-Zuñiga, J. Alloys Compd. **644**, 1003 (2015).
[56] R.-R. Wu, L.-F. Bao, F.-X. Hu, H. Wu, Q.-Z. Huang, J. Wang, X.-L. Dong, G.-N. Li, J.-R. Sun, F.-R. Shen, T.-Y. Zhao, X.-Q. Zheng, L.-C. Wang, Y. Liu, W.-L. Zuo, Y.-Y. Zhao, M. Zhang, X.-C. Wang, C.-Q. Jin, G.-H. Rao, X.-F. Han, and B.-G. Shen, Sci. Rep. **5**, 18027 (2015).
[57] A. Aznar, P. Lloveras, J. Kim, A. A. Avramenko, M. Barrio, J.-L. Tamarit, C. F. Sánchez-Valdés, J. L. Llamazares, N. D. Mathur, and X. Moya, "Giant and reversible inverse barocaloric effects near room temperature in ferromagnetic MnCoGeB0.03," Adv. Mater. (to be published).
[58] L. Mañosa, D. González-Alonso, A. Planes, E. Bonnot, M. Barrio, J.-L. Tamarit, S. Aksoy, and M. Acet, Nat. Mater. **9**, 478 (2010).
[59] J. Rodriguez-Carvajal, T. Roisnel, and J. Gonzales-Platas, FullProf suite (2005 version), Laboratoire Léon Brillouin, CEA-CNRS, CEN Saclay, France, 2005.
[60] Y. Y. Shao, M. X. Zhang, Y. Zhang, A. R. Yan, and J. Liu, J. Magn. Magn. Mater. **362**, 90 (2014).
[61] G. F. Wang, "Magnetic and calorimetric study of the magnetocaloric effect in intermetallics exhibiting first-order magnetostructural transitions," Ph.D. thesis, Prensas Universitarias de Zaragoza, Zaragoza, 2012, pp. 299–233.

[62]W. B. Cui, X. K. Lv, F. Yang, Y. Yu, R. Skomski, X. G. Zhao, W. Liu, and Z. D. Zhang, J. Appl. Phys. **107**, 09A938 (2010).
[63]X. F. Miao, L. Caron, Z. Gercsi, A. Daoud-Aladine, N. H. van Dijk, and E. Brück, Appl. Phys. Lett. **107**, 042403 (2015).
[64]A. Bartok, M. Kustov, L. F. Cohen, A. Pasko, K. Zehani, L. Bessais, F. Mazaleyrat, and M. LoBue, J. Magn. Magn. Mater. **400**, 333 (2016).
[65]E. Brück, O. Tegus, D. T. Cam Thanh, N. T. Trung, and K. H. J. Buschow, Int. J. Refrig. **31**, 763 (2008).
[66]O. Tegus, B. Li-Hong, and S. Lin, Chin. Phys. B **22**, 037506 (2013).
[67]L. Mañosa, D. González-Alonso, A. Planes, M. Barrio, J.-L. Tamarit, I. S. Titov, M. Acet, A. Bhattacharyya, and S. Majumdar, Nat. Commun. **2**, 595 (2011).
[68]S. Yuce, M. Barrio, B. Emre, E. Stern-Taulats, A. Planes, J.-L. Tamarit, Y. Mudryk, K. A. Gschneidner, Jr., V. K. Pecharsky, and L. Manosa, Appl. Phys. Lett. **101**, 071906 (2012).
[69]L. Mañosa, E. Stern-Taulats, A. Planes, P. Lloveras, M. Barrio, J.-L. Tamarit, B. Emre, S. Yüce, S. Fabbrici, and F. Albertini, Phys. Status Solidi B **251**, 2114 (2014).
[70]E. Stern-Taulats, A. Planes, P. Lloveras, M. Barrio, J.-L. Tamarit, S. Pramanick, S. Majumdar, C. Frontera, and L. Mañosa, Phys. Rev. B **89**, 214105 (2014).
[71]E. Stern-Taulats, A. Planes, P. Lloveras, M. Barrio, J.-L. Tamarit, S. Pramanick, S. Majumdar, S. Yüce, B. Emre, C. Frontera, and L. Mañosa, Acta Mater. **96**, 324 (2015).
[72]E. Stern-Taulats, A. Gràcia-Condal, A. Planes, P. Lloveras, M. Barrio, J.-L. Tamarit, S. Pramanick, S. Majumdar, and L. Mañosa, Appl. Phys. Lett. **107**, 152409 (2015).
[73]D. Matsunami, A. Fujita, K. Takenaka, and M. Kano, Nat. Mater. **14**, 73 (2015).
[74]B. Emre, S. Yüce, E. Stern-Taulats, A. Planes, S. Fabbrici, F. Albertini, and L. Mañosa, J. Appl. Phys. **113**, 213905 (2013).
[75]P. Lloveras, E. Stern-Taulats, M. Barrio, J.-L. Tamarit, S. Crossley, W. Li, V. Pomjakushin, A. Planes, L. Mañosa, N. D. Mathur, and X. Moya, Nat. Commun. **6**, 8801 (2015).
[76]A. Aznar, P. Lloveras, M. Romanini, M. del Barrio, J.-L. Tamarit, C. Cazorla, D. Errandonea, N. Mathur, A. Planes, X. Moya, and L. Mañosa, Nat. Commun. **8**, 1851 (2017).
[77]E. Stern-Taulats, P. Lloveras, M. Barrio, E. Defay, M. Egilmez, A. Planes, J.-L. Tamarit, L. Mañosa, N. D. Mathur, and X. Moya, APL Mater. **4**, 091102 (2016).
[78]J. M. Bermúdez-García, M. Sánchez-Andújar, S. Castro-García, J. López-Beceiro, R. Artiaga, and M. A. Señarís-Rodríguez, Nat. Commun. **8**, 15715 (2017).
[79]J. M. Bermúdez-García, S. Yáñez-Vilar, A. García-Fernández, M. Sánchez-Andújar, S. Castro-García, J. López-Beceiro, R. Artiaga, M. Dilshad, X. Moya, and M. A. Señarís-Rodríguez, J. Mater. Chem. C **6**, 9867 (2018).
[80]E. O. Usuda, N. M. Bom, and A. M. G. Carvalho, Eur. Polym. J. **92**, 287–293 (2017).
[81]A. M. G. Carvalho, W. Imamura, E. O. Usuda, and N. M. Bom, Eur. Polym. J. **99**, 212 (2018).
[82]E. O. Usuda, W. Imamura, N. M. Bom, L. S. Paixão, and A. M. G. Carvalho, "Giant reversible barocaloric effects in nitrile butadiene rubber around room temperature," preprint arXiv:1811.01896.
[83]P. Lloveras, A. Aznar, M. Barrio, Ph. Negrier, C. Popescu, A. Planes, L. Mañosa, E. Stern-Taulats, A. Avramenko, N. D. Mathur, X. Moya, and J.-L. Tamarit, Nat. Commun. **10**, 1803 (2019).
[84]S. P. Vallone, A. N. Tantillo, A. M. dos Santos, J. J. Molaison, R. Kulmaczewski, A. Chapoy, P. Ahmadi, M. A. Halcrow, and K. G. Sandeman, Adv. Mater. **31**, 1807334 (2019).
[85]P. E. Markin, N. V. Mushnikov, A. V. Proshkin, and S. V. Belyaev, Solid State Phenom. **190**, 331 (2012).